



Supercapatteries as High-Performance Electrochemical Energy Storage Devices

Linpo Yu¹ · George Zheng Chen^{1,2}

Received: 1 April 2019 / Revised: 19 November 2019 / Accepted: 20 January 2020 / Published online: 26 February 2020
© The Author(s) 2020

Abstract

The development of novel electrochemical energy storage (EES) technologies to enhance the performance of EES devices in terms of energy capacity, power capability and cycling life is urgently needed. To address this need, supercapatteries are being developed as innovative hybrid EES devices that can combine the merits of rechargeable batteries with the merits of supercapacitors into one device. Based on these developments, this review will present various aspects of supercapatteries ranging from charge storage mechanisms to material selection including electrode and electrolyte materials. In addition, strategies to pair different types of electrode materials will be discussed and proposed, including the bipolar stacking of multiple supercapattery cells internally connected in series to enhance the energy density of stacks by reducing the number of bipolar plates. Furthermore, challenges for this stack design will also be discussed together with recent progress on bipolar plates.

Keywords Supercapattery · Supercapacitor · Capacitive and non-capacitive Faradic processes · Nanocomposites · Non-aqueous electrolyte · Device engineering

List of Symbols

C	Capacitance
q	Charge
U	Voltage
i	Current
W	Energy
P	Power
E_g	Energy gap
E	Potential
F	Faraday constant
R	Gas constant
T	Temperature

Abbreviations

EES	Electrochemical energy storage
CVs	Cyclic voltammograms

GCDs	Galvanic charge and discharge plots
EDLCs	Electrical double-layer capacitors
ESR	Equivalent series resistance
Act-Cs	Activated carbons
TMOs	Transition metal oxides
ECPs	Electronically conducting polymers
P α AP	Poly(<i>o</i> -aminophenol)
CNTs	Carbon nanotubes
PANI	Polyaniline
Positrode	Positive electrode
Negatrode	Negative electrode
PPy	Polypyrrole
IL	Ionic liquid
BMPyrrFAP	1-Butyl-1-methylpyrrolidinium tri(pentafluoroethyl)trifluorophosphate
γ -GBL	gamma-Butyrolactone
BMI-TFSI	1-Butyl-3-methylimidazolium bis(trifluoromethylsulfonyl)imide
AQ-PFS ⁻	Perfluorosulfonate anion bearing anthraquinone
TEMPO ⁻ -MI ⁺	Methyl imidazolium cation bearing 2,2,6,6-tetramethylpiperidiny-1-oxyl
NFCS	Non-Faradaic capacitive storage
CFS	Capacitive Faradaic storage
NCFS	Non-capacitive Faradaic storage

✉ George Zheng Chen
george.chen@nottingham.ac.uk
<http://www.nottingham.ac.uk/~enzgzc>

¹ Department of Chemical and Environmental Engineering, Faculty of Science and Engineering, and Key Laboratory of More Electric Aircraft Technology of Zhejiang Province, University of Nottingham Ningbo China, Ningbo 315100, Zhejiang, China

² Department of Chemical and Environmental Engineering, Faculty of Engineering, University of Nottingham, Nottingham NG7 2RD, UK

1 Introduction

Energy derived from intermittent renewable sources such as solar, wind and tide must be stored and supplied in efficient and affordable means to become viable alternatives to traditional non-renewable options. This need has led to the strong desire for energy storage technologies that can be applied to different sustainable energy applications. To address this, researchers have reported that electrochemical energy storage (EES) technologies can be suitable for energy harvesting at various scales and are more attractive than current popular technologies using pumped-storage hydroelectricity, for example [1]. Here, desirable EES devices should possess sufficiently large energy and power capabilities, long cycling lifespans and be commercially affordable. Although rechargeable batteries possess sufficiently large energy capacities, and supercapacitors possess high-power capabilities and long cycle lifespans with great progress being made in both in the past two decades, each technology alone cannot satisfy all the requirements for successful commercialization. To address this, various hybrid EES devices have been proposed and preliminarily demonstrated in which such hybrid devices can combine the merits of supercapacitors with those of rechargeable batteries into one device. However, a unified generic term was lacking for these devices and researchers have generally referred to them using different nomenclatures such as ‘redox capacitors’ [2, 3], ‘Li-ion capacitors’ [4–8], ‘Na-ion capacitors’ [8–10], ‘hybrid electrochemical capacitors’ [11–14], battery–supercapacitor hybrids [15] or ‘pseudocapacitors’ [16–18] corresponding to electrode material and device design and engineering. As a result, a generic term ‘supercapattery’ (= *supercapacitor* + *battery*) was proposed to represent these EES hybrid devices that are different from either supercapacitors or rechargeable batteries in terms of fundamental principles and technological prospects. Since the generic term ‘supercapattery’ was initially proposed in an industrial EES project initiated in 2007, researchers have actively promoted its use, leading to its gradual recognition by the EES community [19–24].

Supercapatteries represent various hybrid EES devices that take advantage of both capacitive and non-capacitive Faradaic (or Nernstian) charge storage mechanisms at either the electrode material level or the device level. For example, Li-ion capacitors possess both a Li-ion battery electrode that can provide non-capacitive Faradaic charge storage and a supercapacitor electrode that can provide capacitive charge storage, meaning that Li-ion capacitors cannot be regarded as a capacitor because of the non-capacitive Faradaic charge storage in the cell nor as a rechargeable battery because of its capacitive behaviour. This is also the case with Na-ion capacitors. Therefore,

‘supercapattery’ as a generic term can be used to describe all devices consisting of a battery electrode and a capacitive electrode such as Li-ion capacitors, Na-ion capacitors and other hybrid EES devices that combine the merits of both capacitive and non-capacitive Faradaic charge storage mechanisms.

Various comprehensive reviews on supercapacitors and supercapatteries as well as critical reviews on electrode materials, electrolytes and engineering fundamentals of supercapatteries have been published in the past 3 years [25–30]. This review, however, intends to introduce the fundamentals of supercapatteries and present recent progress in supercapattery development in terms of electrode and electrolyte materials, device design and engineering and performance advantages and limitations.

2 Fundamentals of Supercapatteries

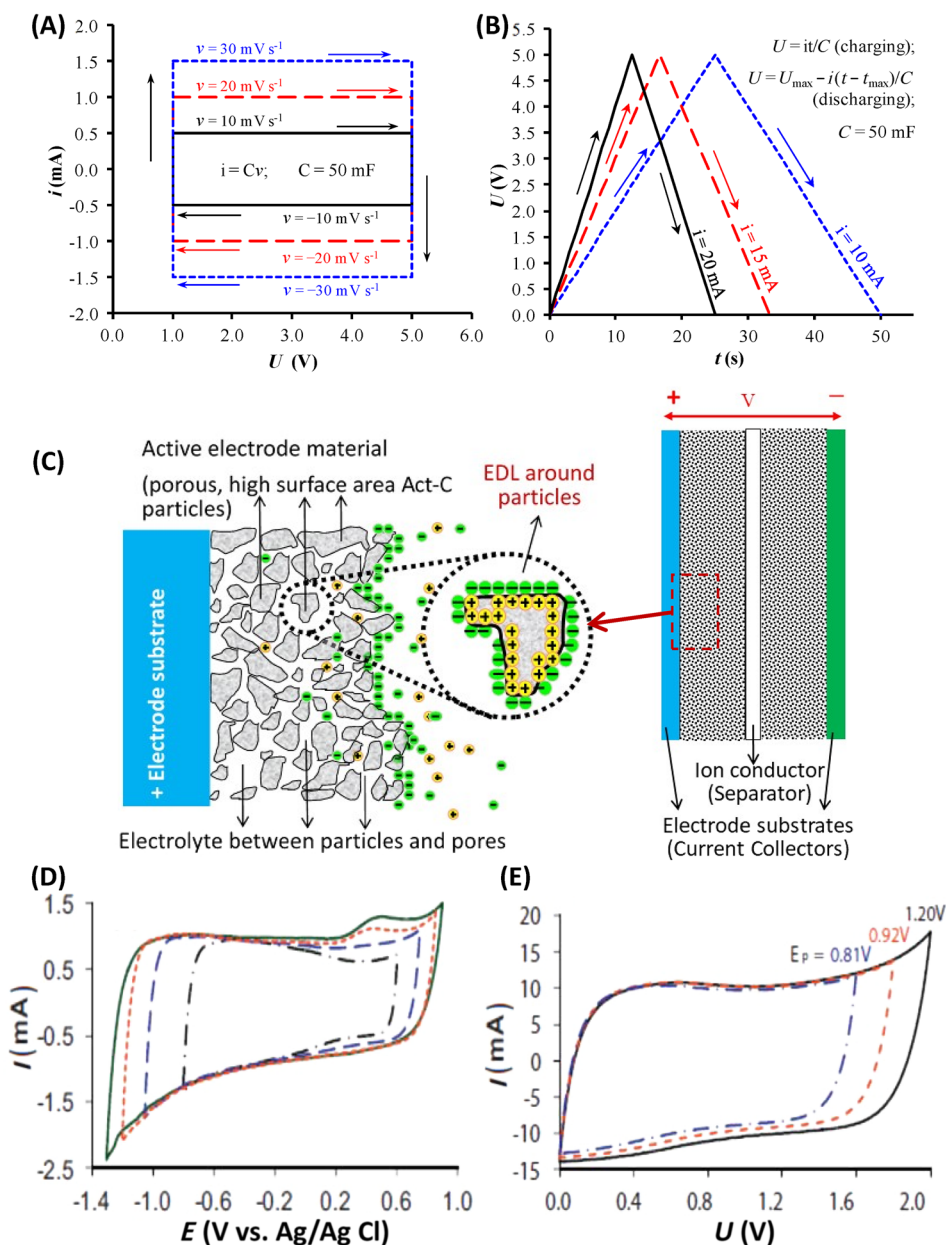
Supercapatteries can exhibit capacitive performances similar to conventional capacitors including rectangular cyclic voltammograms (CVs) and linear galvanic charge and discharge plots (GCDs). Because of this, the fundamentals of conventional capacitors can also be applied to supercapatteries in which capacitance (C) is the proportionality between the stored charge (q) and the voltage (U) applied across a capacitor. This proportionality is also equal to the ratio of the stored charge change (Δq) to the voltage variation (ΔU) as the voltage of a capacitor is scanned at a constant voltage scan rate ($v = dU/dt$) in CVs. Because current (i) flowing through a capacitor is proportional to v , this proportionality is also equal to capacitance as described in Eq. (1).

$$C = \frac{\Delta q}{\Delta U} = \frac{dq/dt}{dU/dt} = \frac{i}{v} \quad (1)$$

For example, the CV of an ideal capacitor as derived from Eq. (1) is 50 mF with a U_{\max} of 5 V (Fig. 1a). In addition, because current at a voltage scan rate remains constant, but current polarity (positive or negative) follows the voltage scan direction (Eq. 1), rectangular-shaped CVs are obtained with sharp current shifts at both ends of the voltage scan. Therefore, CVs can be used to evaluate the capacitive performance of EES devices such as electrical double-layer capacitors (EDLCs), pseudocapacitors and supercapatteries. Furthermore, the CVs of these capacitive EES devices may distort slightly due to the slow kinetics of electrode reactions. Despite this, the ratios of i/v or $\Delta q/\Delta U$ of these devices will remain constant and equal to the capacitance.

Ideal capacitors can also be charged and discharged at constant currents and exhibit triangular GCD plots (Fig. 1b) in which as these capacitors are charged, U will

Fig. 1 **a** CVs at indicated cell voltage scan rates and **b** GCD plots at indicated constant currents of a hypothetical conventional capacitor of $C = 50$ mF with $U_{\max} = 5$ V derived from Eq. (1) [27, 30, 31]. **c** Schematic illustration of the charge storage mechanism in an EDLC using Act-C electrodes. The enlarged view in the point cycle shows charge storage on a single carbon particle through ion adsorption at the carbon–electrolyte interface (i.e. EDL capacitance) [30]. CVs of **d** Act-C in $0.3 \text{ mol L}^{-1} \text{ K}_2\text{SO}_4$ at 5 mV s^{-1} in different potential ranges and **e** a symmetrical cell with equal amounts of Act-C on each electrode and $0.3 \text{ mol L}^{-1} \text{ K}_2\text{SO}_4$ as the electrolyte at 5 mV s^{-1} in decreasing voltage ranges [32]



build up across the positive and negative electrodes. Here, Eq. (2) can be used to calculate the energy (W) stored by a capacitor and indicates that W is proportional to the capacitance of the cell (C_{cell}) and the square of ΔU .

$$W = \frac{1}{2} C_{\text{cell}} \Delta U^2 \tag{2}$$

It should be noted that W must be calculated through the integration of GCD plots in the discharge portion as described in Eq. (3) and is applicable to all EES devices,

whereas Eq. (2) is a special case in which GCD plots in the discharge portion are linear (Fig. 1b).

$$W = \int_0^t iUdt = i \int_0^t Udt \tag{3}$$

Another important factor for capacitors is the maximum power output (P_{\max}), which can only be reached if the working load resistance is equal to the equivalent series

resistance (ESR) of a capacitor. Equation (4) shows the relationship between P_{\max} , U and ESR.

$$P_{\max} = \frac{U^2}{4\text{ESR}} \quad (4)$$

Conventional capacitors usually possess small capacitances in the range of 10^{-6} – 10^{-2} F such as the 50 mF capacitance capacitor (Fig. 1a, b), meaning that even if U can be charged to 100 V, energy capacities can only reach 2500 J (~ 0.7 Wh) for this capacitor. Alternatively, the capacitance of supercapacitors can easily reach greater than 100 F. Despite these differences in capacitance, however, both capacitors and supercapacitors possess EDL charge storage mechanisms, and currently, the most widely used supercapacitor materials are high surface area activated carbons (Act-Cs) (Fig. 1c).

For example, Chae et al. [32] investigated Act-Cs as a supercapacitor electrode and reported that Act-Cs can retain rectangular CVs at different potential ranges (Fig. 1d), indicating an EDL storage mechanism in which as the potential range gradually extended, cathodic and anodic reactions appeared at -1.1 V and 0.5 V versus Ag/AgCl, respectively. Here, these researchers attributed the reduction reaction to $\text{H}^+ + \text{e} \rightarrow \text{H}_{\text{ad}}$ in the micropores of Act-Cs and reported that the reductive potential was more negative than the theoretical negative potential limit for water (-1.0 V vs. Ag/AgCl) [33], suggesting that such negative reductive potentials were mainly due to the overpotential of carbon-based materials. A small anodic current hump at 0.5 V (Fig. 1d) was also observed and was interpreted as evidence of the re-oxidation of produced H_{ad} in the micropores of Act-Cs. These researchers also reported that as the potential range was further extended (more positive than 0.9 V vs. Ag/AgCl), a further oxidation current at potentials beyond 0.8 V was observed, which was attributed to the oxidation of water $\text{H}_2\text{O} = \text{O}_2 + 4\text{H}^+ + 4\text{e}$ [34] and/or carbon $\text{C} + \text{H}_2\text{O} = \text{CO}_2 + 4\text{H}^+ + 4\text{e}$ [32]. Furthermore, the Act-Cs in this study exhibited satisfactory capacitive performances in both positive and negative potential scans between positive and negative limits in which a symmetrical supercapacitor with equal amounts of Act-Cs on each electrode was fabricated (Fig. 1e) and the obtained cell voltage easily reached 1.9 V or even higher due to the wide capacitive potential range of the Act-Cs in aqueous electrolytes.

In general, the specific capacitance of electrode materials (C_{sp}) can easily be derived from relevant CVs. By considering the fact that equal amounts of electrode materials ($m_+ = m_- = m$) are used to fabricate symmetrical supercapacitors, the specific capacitance and specific energy of cells ($C_{\text{sp,cell}}$ and W_{sp}) can be expressed as the ratios of C_{cell} and W to the total mass of the electrode material ($m_+ + m_- = 2m$),

respectively, in which $C_{\text{sp,cell}} = \frac{1}{2m}C_{\text{cell}} = \frac{1}{4}C_{\text{sp}}$ and $W_{\text{sp}} = W/2m$. And by considering Eq. (2) in these relationships, W_{sp} can be rearranged as Eq. (5).

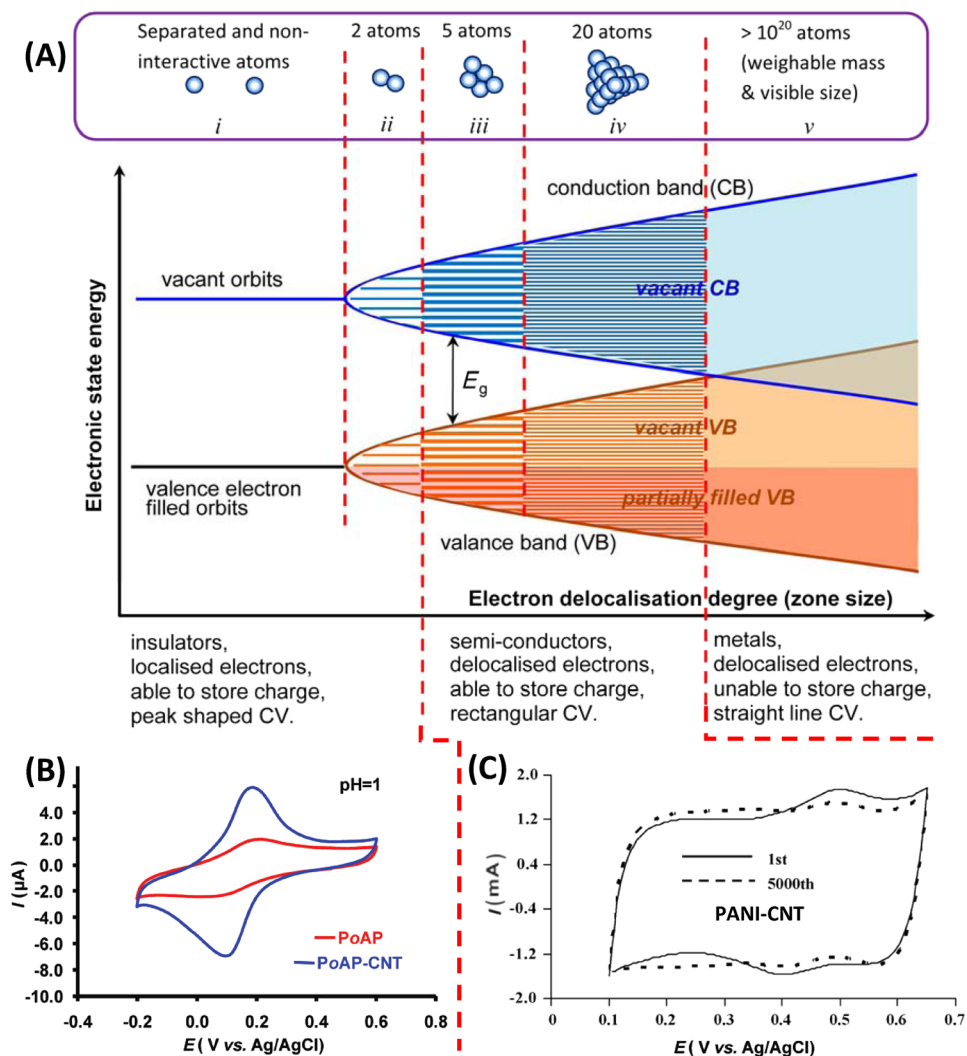
$$W_{\text{sp}} = \frac{\frac{1}{2}C_{\text{cell}}\Delta U^2}{2m} = \frac{1}{8}C_{\text{sp}}\Delta U^2 \quad (5)$$

The above equations are also applicable to pseudocapacitors and supercapacities, both of which exhibit rectangular CVs and linear GCD plots. Here, transition metal oxides (TMOs) and electronically conducting polymers (ECPs) have both been widely used as pseudocapacitive materials that can provide capacitive Faradaic charge storage from the transfer of delocalised valence electrons. Using metal clusters with different sizes as examples (Fig. 2a), the delocalisation of valence electrons corresponds to energy levels in which as more atoms are bound to clusters, orbits will split into more sub-orbits, leading to smaller energy gaps between the neighbouring energy levels of sub-orbits. And if the energy gap (E_g) between the lowest energy level of the higher energy group and the highest energy level of the lower energy group is large enough, all valence electrons will occupy the energy levels of the lower energy group, leaving higher energy levels empty, meaning that these valence electrons are localised at these lower energy levels. Here, if materials possessing these localised electrons are used to store charge, the Nernst equation (Eq. 6) [35] will govern reactions at a potential range near the equilibrium potential E^0 , leading to current peaks on CVs and potential plateaus on GCD plots.

$$E = E^0 + \frac{nF}{RT} \ln\left(\frac{1-x}{x}\right) \quad (6)$$

Here, n is the number of electrons transferred, F is the Faraday constant, R is the gas constant, T is the temperature, and x is the mole fraction of the reduced species or sites. As an example of localised charge storage, Hu et al. [36] reported peak-shaped CVs from a non-conducting polymer, poly(*o*-aminophenol) (PoAP), with and without carbon nanotubes (CNTs) in an acidic electrolyte (Fig. 2b) in which PoAP was non-conductive and can provide localised electrons for charge storage. In addition, TMOs and ECPs are semiconductors with delocalised electrons that can easily move between occupied and unoccupied orbits within valance bands (Fig. 2a) in which the difference of energy levels or potentials between neighbouring orbits is so small that every small potential variation will cause electron transfer, leading to constant currents with linear variations of potential in a capacitive manner the same as in EDLCs. Furthermore, Peng et al. [37] also reported that the polyaniline-CNT (PANI-CNT) composite, a type of

Fig. 2 **a** Schematics of charge storage mechanisms based on localised and delocalised electrons and relevant split energy levels [27]. **b** Localised charge storage with peak-shaped CVs recorded from PoAP (red) and PoAP-CNT (blue) in 1 mol L⁻¹ HCl at 10 mV s⁻¹ [36]. **c** CVs of PANI-CNT composite recorded in the first and the 5000th potential scan cycles in 1.0 mol L⁻¹ HCl at 100 mV s⁻¹ [37]



ECP composite, can demonstrate rectangular CVs within a capacitive potential range (Fig. 2c).

In summary, three charge storage mechanisms exist in supercapacitors. The first mechanism involves EDL capacitance, which stores charge on electrode surfaces reversibly. The second mechanism is the Nernstian process, also called the non-capacitive Faradaic process, which broadly follows the Nernst equation describing the transfer of localized valence electrons. The third mechanism involves pseudocapacitance and is also called the capacitive Faradaic process, which proceeds in the capacitive pathway based on the transfer of delocalized valence electrons. Here, all three charge storage mechanisms can be applied to electrode materials for supercapacitors.

The specific energy of EDLCs has a strong relationship with the maximum charging voltage and specific capacitance. As for TMOs and ECPs, these are pseudocapacitive materials because of their semiconductor nature and possess higher specific capacitances than EDLCs but narrower

potential ranges. Due to this, symmetrical devices composed of pseudocapacitive materials are not favourable for high energy capacity EES devices and various asymmetrical designs have been proposed to achieve high voltage. Currently, two main designs for asymmetrical devices exist in which one involves asymmetrical supercapacitors with positive and negative electrodes (the positrode: the positive electrode [24, 27, 38–43]; the negatrode: the negative electrode [24, 27, 39–44]) capable of capacitive charge storage typically through the permutation and combination of EDL and pseudocapacitive electrodes, whereas the other design involves hybrid configurations that combine supercapacitor electrodes with battery electrodes and have been reported under different names that mainly correspond to the different electrode materials used. Overall, the word ‘hybrid’ is not a suitable unified expression for the future development of these asymmetrical devices because it is too abstract, whereas the terms ‘supercapacitor’ or ‘supercapattery’ are general enough to represent

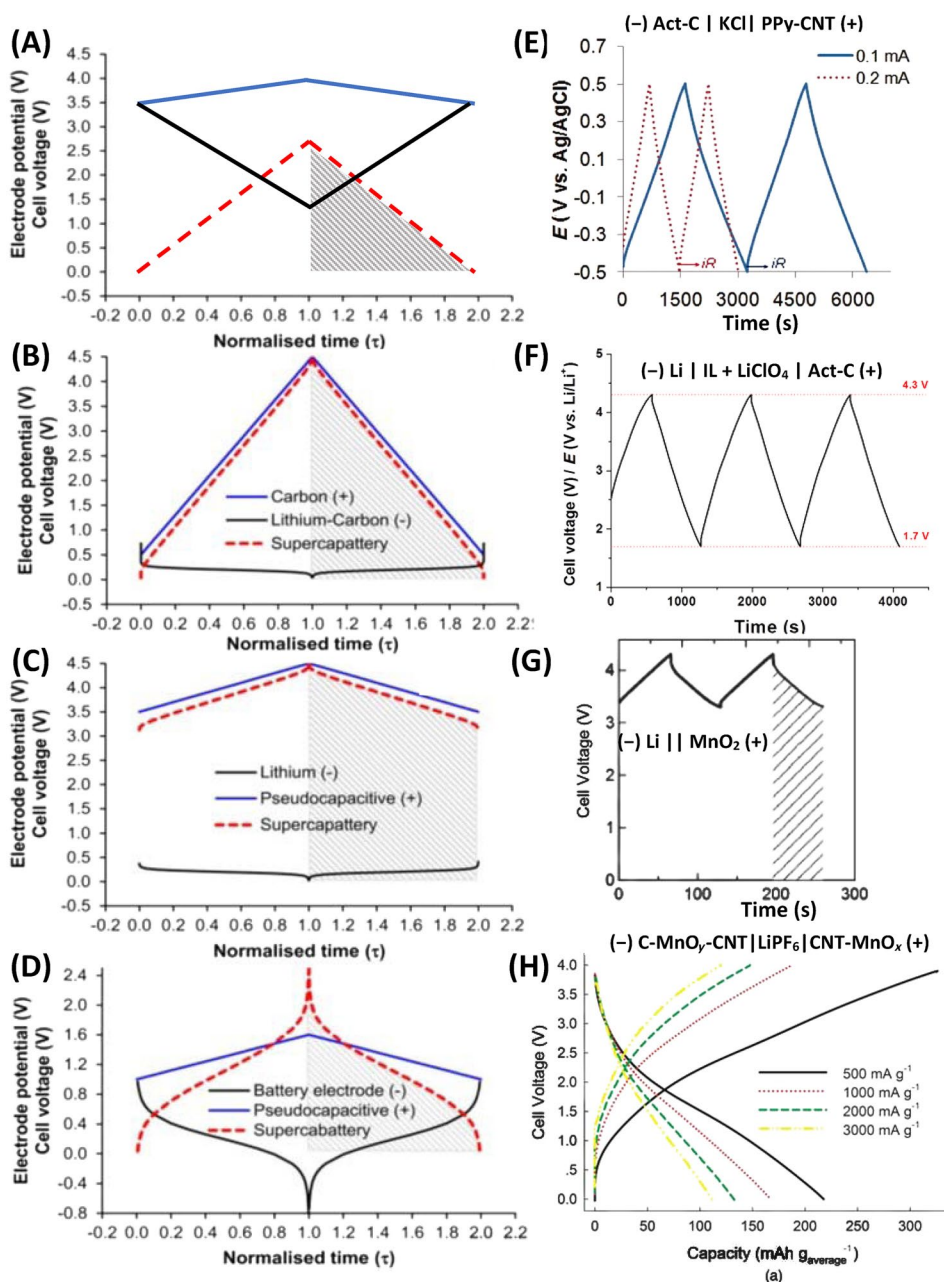
these asymmetrical devices vividly. And because supercapacitors take advantage of Faradaic charge storage in typical non-capacitive Faradaic storage, pseudocapacitors also fall in the scope of supercapacitors in a broad sense. And more often, supercapacitors contain electrodes with battery-type charge storage.

3 Materials for Supercapacitors

3.1 Electrode Materials

Electrode materials with EDL capacitance, pseudocapacitance or the Nernstian process can be utilised in supercapacitors in which different types of electrode materials will result in different supercapacitors. In order to comprehensively discuss these hybrid devices, several hypothetical supercapacitors were constructed by us [27] to illustrate their performance by using corresponding GCD plots one by one (Fig. 3a–d) and these hypothetical devices were

Fig. 3 Calculated GCD plots of positrodes (blue lines), negatrodes (black lines) and relevant cells (red dash lines): **a** a hypothetical pseudocapacitor with an Act-C negatrode and a pseudocapacitive positrode and a hypothetical supercapattery with a negatrode of Li metal or lithiated carbon and **b** an Act-C positrode or **c** a pseudocapacitive positrode [27]. **d** A hypothetical supercapattery with a typical battery-type negatrode and a pseudocapacitive positrode [27]. **e** Experimental demonstration of **(a)**, (-) Act-C | KCl | PPy-CNT (+) [45]. **f** Experimental demonstration of **(b)**, (-) Li | IL + LiClO₄ | Act-C (+) [23]. **g** Experimental demonstration of **(c)**, (-) Li | PEO-LiTFSI | LTAP | 1.0 M LiCl aq. | MnO₂ (+) [12] (Reproduced with permission from Ref. [12]; permission conveyed through Copyright Clearance Center, Inc.). **h** Experimental demonstration of **(d)**, (-) C-MnO_x-CNT | LiPF₆ | MnO_x-CNT (+) [22] (Reproduced with permission from Ref. [22]; permission conveyed through Copyright Clearance Center, Inc.)



confirmed by using relevant experimental data from the literature (Fig. 3e–h).

The first hypothetical supercapattery that was considered was a pseudocapacitor consisting of a pseudocapacitive positrode and an EDL capacitance negatrode. Here, the capacitive potential range of the pseudocapacitive positrode was relatively narrow (3.5–4.0 V), whereas the EDLC negatrode operated from 1.5 to 3.5 V to match the charge stored by the positrode with the predicted behaviour of the electrodes and the cell being demonstrated by GCD plots (Fig. 3a). And because the balance of electrode mass and charge is important for all EES devices, the amount of charge passing through the positrode must be equal to the charge passing through the negatrode in a supercapattery. Based on this, the mass, specific capacitance, voltage variation and amount of stored charge of positrodes and negatrodes must follow Eq. (7)

$$q_- = m_- C_{sp-} \Delta U_- = m_+ C_{sp+} \Delta U_+ = q_+ \quad (7)$$

where q represents the amount of charge passing through the electrode, m is the mass of the electrode, and the subscripts – and + represent the negatrode and the positrodes, respectively. As for the hypothetical pseudocapacitive positrode and the EDLC positrode, $C_{sp,pseudo}$ of 500 F g^{-1} and $C_{sp,EDLC}$ of 200 F g^{-1} were hypothesis. Furthermore, by rearranging Eq. (7) and using available values, the mass ratio of the positrode to the negatrode in the hypothetical pseudocapacitor was calculated to be $m_{pseudo}/m_{EDLC} = C_{sp,EDLC} \Delta U_- / C_{sp,pseudo} \Delta U_+ = \frac{500 \times 0.5}{200 \times 2} = 0.625$ with $C = 1/2 \times (1/(0.625 \times 500) + 1/200) = 61 \text{ F g}^{-1}$. Equation (5) can also be applied to calculate the specific energy of this hypothetical pseudocapacitor because the performance of the hypothetical cell is capacitive, leading to a value of 53 Wh kg^{-1} , which is higher than values obtained from a symmetrical EDLC ($W_{sp,sym} = 43 \text{ Wh kg}^{-1}$) with the same ΔU .

Another hypothetical supercapattery hypothesised in this study was a common supercapattery possessing a Li metal negatrode and an Act-C positrode. Here, based on the behaviour of the electrodes and the cell as shown by GCD plots (Fig. 3b), the behaviour of this hypothetical cell was highly capacitive, meaning that Eq. (5) can be used to calculate the corresponding energy capacity. The minimum potential of the Act-C positrode was also set to 0.5 V vs. Li/Li⁺ to prevent the lithiation of the Act-C electrode during discharge. Furthermore, the mass of the positrode and the negatrode in this hypothetical supercapattery can be represented based on the charge passing through based on Eq. (8)

$$Q_- = m_- Q_{sp-} = m_+ C_{sp+} \Delta E_+ = Q_+ \quad (8)$$

Here, $Q_{sp,Li} = nF/M_{Li} = 13900 \text{ C g}^{-1} = 3861 \text{ mAh g}^{-1}$ for the Li metal negatrode in which $n = 1$, $F = 96485 \text{ C mol}^{-1}$

and $M_{Li} = 6.941 \text{ g mol}^{-1}$, whereas for the Act-C positrode, $C_{sp,C} = 200 \text{ F g}^{-1}$ and $\Delta U = 4.0 \text{ V}$ were hypothesised. And by taking into account all of the data in Eq. (8), the mass ratio of the positrode to the negatrode can be calculated to be $m_C/m_{Li} = Q_{sp,Li}/C_{sp,C} \Delta E = \frac{13900}{200 \times 4.0} = 17.4$. And because the ratio was so high, the mass of the Li metal negatrode was negligible as compared with that of the Act-C positrode in the supercapattery, whose capacitance value was approximately equal to the capacitance value of the Act-C positrode. Furthermore, because the minimum potential of the Act-C electrode was set to 0.5 V versus Li/Li⁺ instead of zero, then $\Delta U^2 = (4.5 \text{ V})^2 - (0.5 \text{ V})^2$. Moreover, according to Eq. (5), the above data lead to $W_{sp} = 555.6 \text{ Wh kg}^{-1}$, which was much higher than that of the pseudocapacitor.

Another hypothetical supercapattery was constructed by replacing an EDLC positrode with a pseudocapacitive electrode (Fig. 3c) in which the specific capacitance of the pseudocapacitor electrode was assumed to be 500 F g^{-1} and the potential range of ΔE was assumed to be 1.0 V because pseudocapacitive materials are perceived to possess high specific capacitance and narrow potential range. Based on this, the mass ratio was calculated to be $m_C/m_{Li} = Q_{sp,Li}/C_{sp,C} \Delta E = \frac{13900}{500 \times 1.0} = 27.8$, again indicating that the mass of the negatrode was negligible in the supercapattery. Similarly, by using $C_{sp,cell} \approx C_{sp,C} = 500 \text{ F g}^{-1}$, $U_{max} = 4.5 \text{ V}$ and $U_{min} = 3.5 \text{ V}$ in Eq. (5), the specific energy of this hypothetical cell was calculated to be 555.6 Wh kg^{-1} , which is equal to the value of the previous hypothetical supercapattery. Here, because Li metal electrodes work reversibly at negative potentials (Fig. 3b, c), sluggish curves can commonly be observed in the GCD plots of most battery electrodes (Fig. 3d). And because this hypothetical device consisted of a pseudocapacitive positrode and a battery negatrode, the battery negatrode charged/discharged at a more positive potential and the corresponding GCD plot was more sluggish as compared with the Li metal negatrode. In addition, the GCD plot of this hypothetical device was not linear in either the charge or the discharge portion, meaning that the performance of this device was not capacitive. As a result, the GCD of the cell was integrated to evaluate the cell energy capacity by using Eq. (3) instead of Eq. (2). Moreover, the shadowed area under the discharge branch of the GCD plots was proportional to the energy capacity of the cell in which the GCD plot (Fig. 3d) was more like that of a battery, meaning that the term ‘supercapattery’ is more appropriate for this hypothetical device.

Experimentally (Fig. 3e–h), Zhou et al. [45] reported that a supercapattery consisting of a polypyrrole-CNT (PPy-CNT) composite positrode, an Act-C negatrode and a 3 mol L^{-1} KCl electrolyte can exhibit typical capacitive behaviours (Fig. 3e). Furthermore, Yu et al. [23] successfully demonstrated another supercapattery consisting of an Act-C positrode and a Li/Li⁺ negatrode in an ionic liquid

(IL) electrolyte consisting of 1-butyl-1-methylpyrrolidinium tri(pentafluoroethyl)trifluorophosphate (BMPyrrFAP), gamma-butyrolactone (γ -GBL) and LiClO_4 and reported that the IL solution not only provided cations and anions for non-Faradic capacitive storage at the Act-C surface, but also enabled Li/Li^+ redox reactions on the negatrod for non-capacitive Faradic or Nernstian storage. In addition, these researchers reported that the GCD plot of this supercapattery demonstrated typical capacitive GCD features (Fig. 3f) and that the resulting specific energy reached 230 Wh kg^{-1} at 1 mA cm^{-2} (based on active materials), which is the highest recorded for supercapatteries consisting of Act-C electrode materials. Makino et al. [12] also investigated a cell composed of (-) $\text{Li} \mid \text{PEO-LiTFSI} \mid \text{LTAP} \mid 1.0 \text{ mol L}^{-1} \text{ LiCl}$ (60°C) $\mid \text{MnO}_2$ (+) in which PEO-LiTFSI acted as a buffer layer and LTAP as a solid electrolyte made of LISICON-type solid glass ceramics. Here, the obtained GCD plot (Fig. 3g) was similar to the calculated hypothetical GCD plot (Fig. 3c), indicating the validity of the hypothetical cells and corresponding equations. Furthermore, Zhou et al. [22] experimented on a typical supercabattery composed of MnO_x -CNT composites (Fig. 3h) and reported calculated specific energy of 208.6 Wh kg^{-1} using Eq. (3), of which 105.8 Wh kg^{-1} remained under ultrahigh specific power of 3000 W kg^{-1} .

Based on these experimental studies, pseudocapacitive materials composed of TMO and ECP composites can play vital roles in the engineering of electrode materials for supercapatteries. Here, researchers have reported that CNTs are suitable for the construction of these composites in situations requiring porous structures for the transportation of charge balancing ions. Furthermore, CNTs possess high electrical conductivity and can therefore improve the electrical conductivity of composites. For example, Jin et al. [46] studied the two-stage progress of MnO_2 redox deposition on CNTs due to the effects of nanoscaled micro-electrochemical cells. Here, these researchers reported that at the beginning stage of the redox deposition (Fig. 4a), MnO_2 precipitation can only be found at or near the defect sites of CNTs as evidenced by TEM images of the MnO_2 -CNT composite (Fig. 4c) and that at a later stage (Fig. 4b), the electrically conductive CNTs created defects and other locations on the CNT wall as the anode and the cathode, respectively. These researchers also suggested that electron transfer in the micro-electrochemical cell can promote the growth of MnO_2 away from defects (e.g. inside the cavity of CNTs, Fig. 4d) and that this mechanism not only applies to MnO_2 -CNT composites, but also applies to composites of various TMOs and other carbon-based nanomaterials such as graphene and silicon carbide.

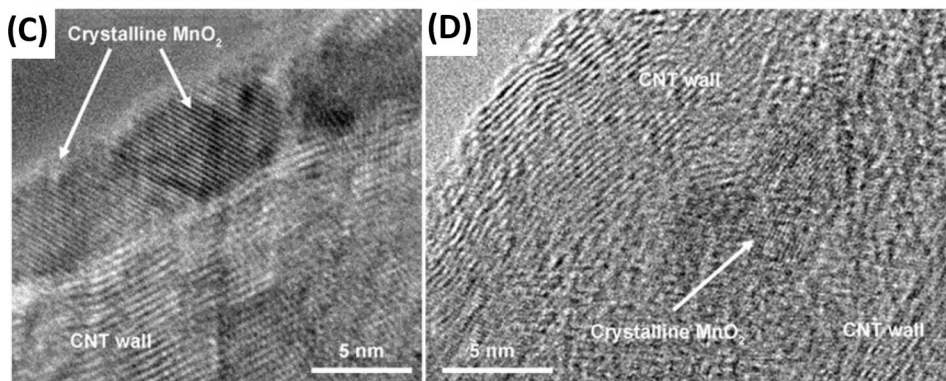
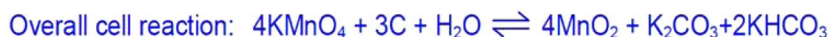
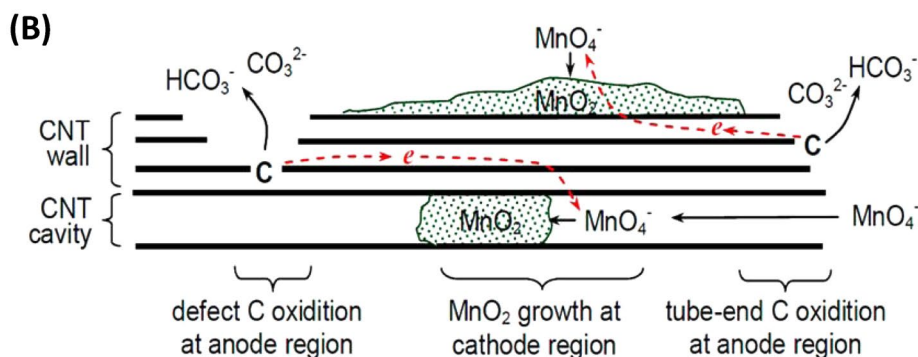
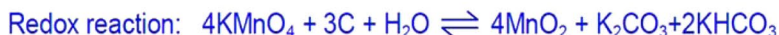
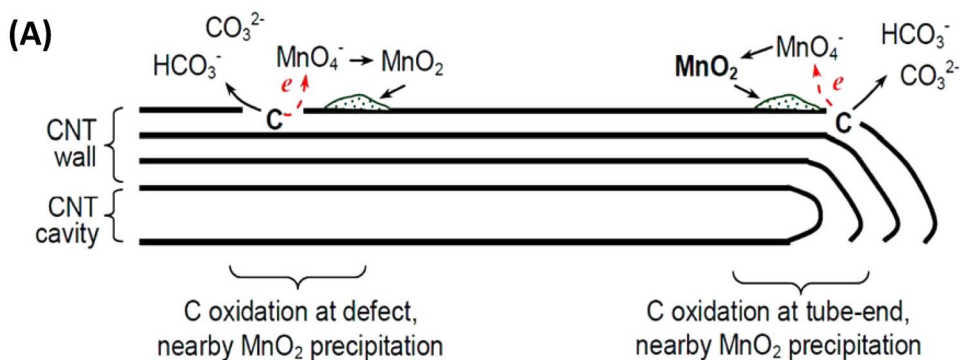
3.2 Electrolytes

Electrolytes are an indispensable component in all types of EES devices and allow for the transportation of ions to achieve ionic conductivity and the maintenance of electronic insulation between positrodes and negatrododes. In the case of supercapatteries, electrolytes also provide redox ions for electrode reactions (Fig. 2). More recently, electrolytes with additional redox species have attracted increasing attention because these redox electrolytes in supercapatteries can significantly enhance energy capacity [24, 47–49].

As an example of an IL electrolyte comprising of bi-redox species for the enhancement of supercapattery energy capacities, Mourad et al. [50] mixed an IL composed of 1-butyl-3-methylimidazolium bis(trifluoromethylsulfonyl)imide (BMI-TFSI) with another bi-redox IL composed of the perfluorosulfonate anion bearing anthraquinone (AQ-PFS⁻) and the methyl imidazolium cation bearing 2,2,6,6-tetramethylpiperidiny-1-oxyl (TEMPO-MI⁺) and used this IL mixture (Fig. 5a) as the electrolyte in a capacitive EES device composed of EDCL electrodes. Here, these researchers postulated that the cations and anions in the BMI-TFSI can be drawn into the negatrod and the positrod, respectively, and be adsorbed on carbon surfaces without invoking any Faradaic reactions during supercapacitor charging. Alternatively, these researchers also suggested that as the redox-active AQ-PFS⁻ and TEMPO-MI⁺ are electro-adsorbed on the surface of EDLC electrodes, redox species will undergo fast Faradaic reactions. Serious self-discharging can occur in EES devices if redox species are dissolved in electrolytes, especially for electrolytes in supercapacitors. However, in the case of the mixture of bi-redox IL and BMI-TFSI, this issue appeared to have been avoided by the bulky size and high viscosity of the IL. Mourad et al. [50] in the same study also used Act-Cs (from PICA) and the bi-redox IL to fabricate a supercapacitor and studied the CVs of the carbon-based symmetrical supercapacitor with 0.5 mol L^{-1} AQ-PFS⁻ and TEMPO-MI⁺ in BMI-TFSI as compared with neat BMI-TFSI at 5 mV s^{-1} (Fig. 5b). And because micropores and mesopores in PICA can restrict access for IL ions, these researchers reported that the current amplitude in the CVs of the resulting supercapacitor doubled as the electrolyte changed from BMI-TFSI to the 0.5 mol L^{-1} bi-redox IL. These researchers also reported that the broad oxidation and reduction peaks in the CVs appeared at intermediate voltages and attributed this to the redox processes of the bi-redox IL in the supercapacitor.

Akinwolemiwa et al. [24] recently also conducted another study into redox electrolytes in which the electrochemical behaviour of dissolved redox species in electrolytes and supercapattery features from the standpoint of Act-C electrode EDL capacitance was investigated. Here, based on the CVs and GCD plots of an equal electrode mass bi-electrolyte

Fig. 4 Schematics of the redox deposition of MnO₂ on CNTs in two stages: **a** Stage 1: direct redox deposition of MnO₂ near the defect on CNTs. **b** Stage 2: nanoscale micro-electrochemical cell-induced cathodic reaction to further grow a coating of MnO₂ on the external or the internal surface of CNTs. TEM images of **c** crystalline MnO₂ coating on a CNT and **d** the cavity of a CNT filled with crystalline MnO₂ [46]



cell (–) Act-C | 2.0 mol L⁻¹ KOH || 2.0 mol L⁻¹ KI | Act-C (+) (Fig. 6a, b), these researchers reported that the CV current flow increased at high cell voltages from 0.8 to 1.5 V and that the redox reaction of KI did not contribute to charge storage in the negatrode, demonstrating a method to achieve current peaks at high cell voltages in supercapatteries with dissolved redox species.

In summary, dissolved redox species such as the bi-redox IL and KI can increase the energy capacity of supercapatteries by storing significant amounts of charge and by retaining redox species in electrode pores or near electrodes. A more detailed discussion concerning the contribution of dissolved redox species in electrolytes to energy capacity can be found in a previous review [47].

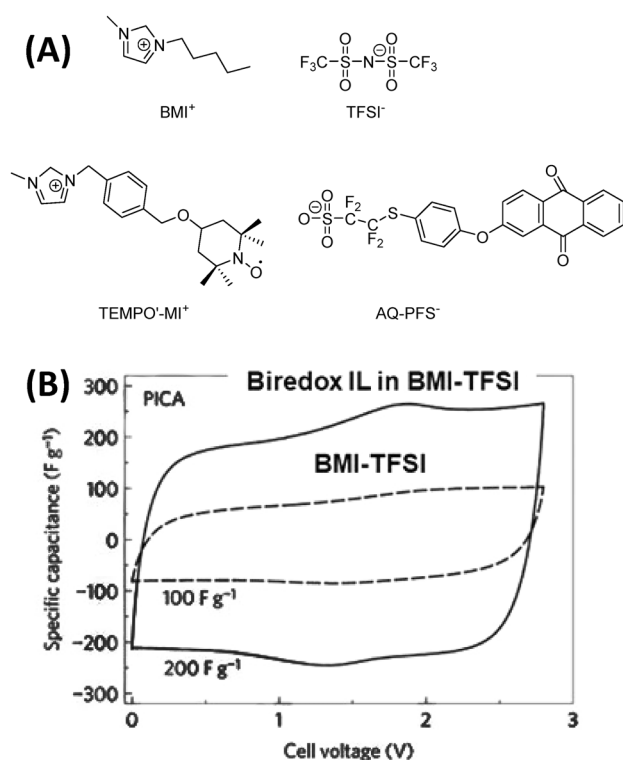


Fig. 5 **a** Molecular structures of BMI-TFSI and the bi-redox IL with the anthraquinone and 2,2,6,6-tetramethylpiperidiny-1-oxyl group. **b** CVs of supercapacitors composed of PICA (Act-Cs) electrodes at 5 mV s^{-1} with the 0.5 mol L^{-1} bi-redox IL in BMI-TFSI (the solid line) and pure BMI-TFSI (the dashed line) [50]. (Reproduced with permission from Ref. [50]. Copyright © 2016, Springer Nature)

4 Device Engineering

Electrode materials, especially TMO and ECP composites, are usually in the powder form unless electrodeposited on electrodes [51, 52]. Due to this, various methods have been applied to fabricate electrodes. For example, Zhou et al. [53] successfully screen-printed chemically synthesised ECP-CNT composites onto titanium plates to produce supercapattery electrodes including stable ink and thick screen-printed Act-C and PPy-CNT electrodes (Fig. 7a–c) and assembled two pieces of the screen-printed electrodes into a supercapattery (Fig. 7d), resulting in high IR drops being observed in the obtained GCD plots (Fig. 7e). Here, these researchers used titanium plates because they can be used as both current collectors and bipolar plates to reduce the weight of stacks with multiple supercapatteries. And although the supercapattery in this study with the screen-printed electrodes operated properly, challenges for these screen-printed electrodes exist, including the lack of suitable current binders and surfactants for ink. This is because a high mass ratio of binders and surfactants needs to be added into the ink to

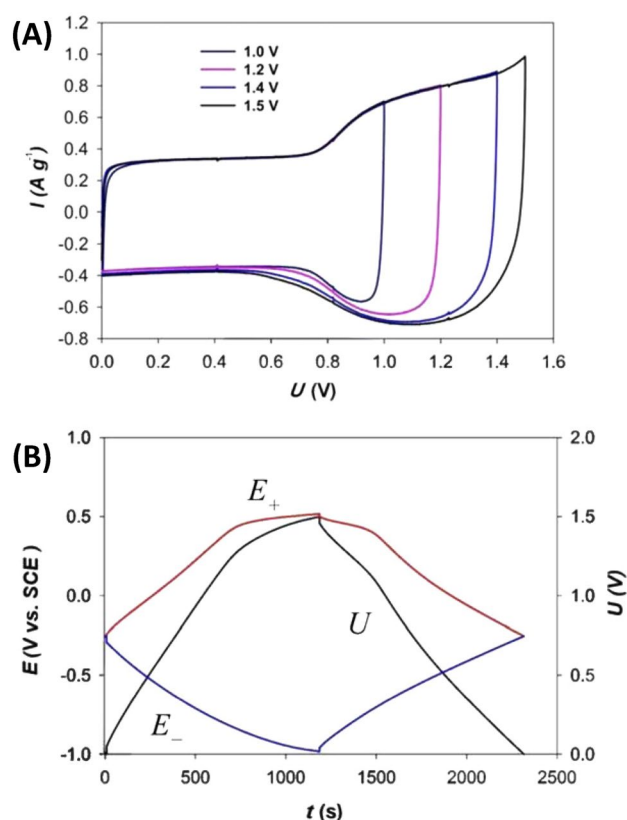


Fig. 6 **a** CVs of an equal electrode mass bi-electrolyte cell (–) Act-C | 2.0 mol L^{-1} KOH || 2.0 mol L^{-1} KI | Act-C (+) at 5.0 mV s^{-1} with different upper limits of cell voltage. **b** GCD plots of the same cell with a 1.5 V upper limit of cell voltage at 0.1 A g^{-1} [24]

produce strong, thick printed layers, which increases resistivity as compared with electro-co-deposited ECP-CNT composites. Furthermore, the thickness of screen-printed electrodes needs to be more adjustable. Another approach reported by researchers is to fabricate composite electrodes with fewer binders or without binders.

The bipolar stacking is another effective engineering design to fabricate supercapatteries in which neighbouring supercapattery cells are connected in series by bipolar plates in the stack (Fig. 8a), allowing almost half of the titanium plate to be removed as compared with ones fabricated by using external cable connections (required the titanium plate number: $n + 1$ vs. $2n$, n = the number of the cells). As an example of the bipolar stacking, Zhou et al. [45] fabricated 19 single cells with the configuration of (–) Ti | CMPB | 0.5 mol L^{-1} KCl | PPy-CNT | Ti (+) in which Ti is the titanium bipolar plate and CMPB is Cabot Monarch 1300 pigment black, which is a specialty Act-C. Here, PPy-CNT composites were mixed with only 5 wt% polyvinyl alcohol as the binder in the positrode and the resulting GCD plots exhibited negligible IR drops at all GCD

Fig. 7 Photographs of **a** the ink of the PPy-CNT composite, **b** the screen-printed electrode with Act-Cs on the titanium plate and **c** the screen-printed electrode with the PPy-CNT composite on the titanium plate. **d** Schematic of a unit cell with the screen-printed electrodes. **e** GCD plots of the unit cell at different currents [53]

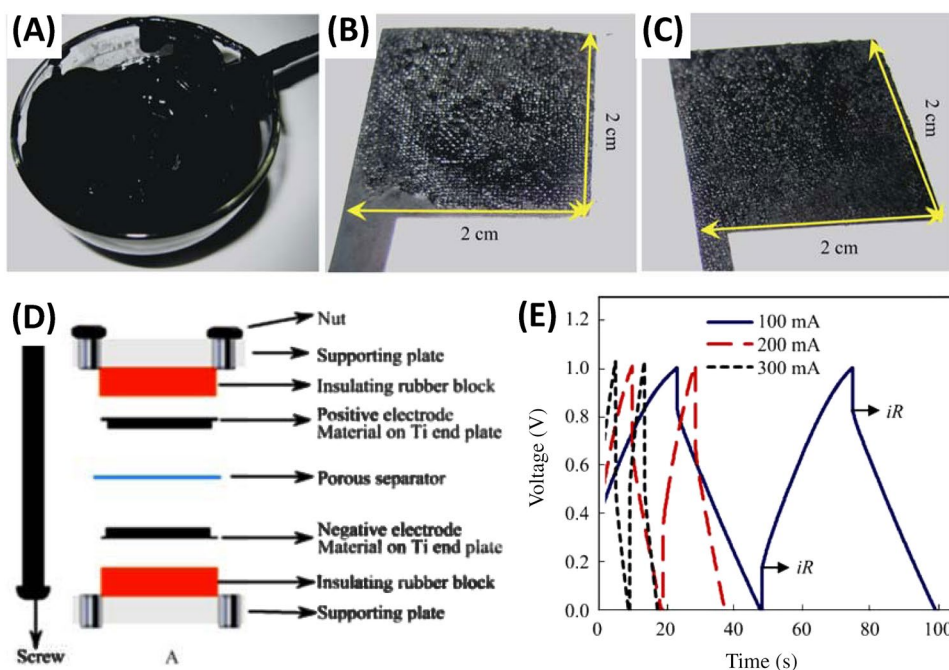
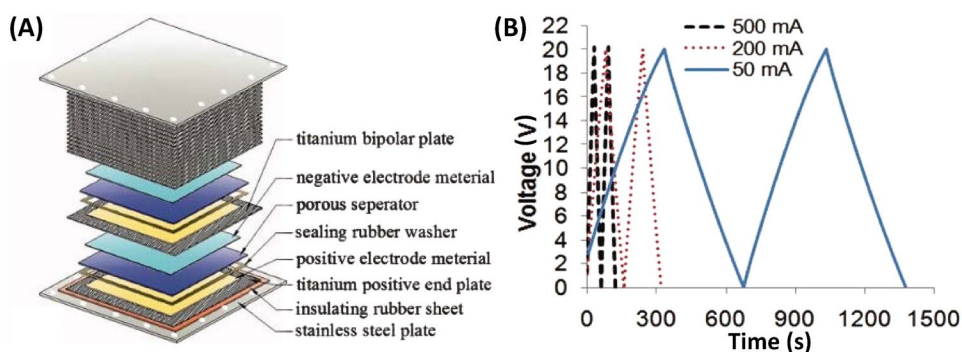


Fig. 8 **a** Expanded schematic of a bipolar stack of 19 supercapacitors. **b** Corresponding GCD plots of the stack [45]



currents (Fig. 8b). These researchers also reported that the minimum ESR detected by electrochemical impedance spectroscopy was only 0.3 Ω and that according to Eq. (4), $P_{\max} = \frac{U^2}{4ESR} = 333 \text{ W}$ or 24 W g^{-1} against the total mass of the active materials.

And although laboratory demonstrations of the 19-cell stack have proven the feasibility of the bipolar stacking in scalable EES devices, the main concern of bipolar plates is the balance between plate weight and permeability. This is because permeability is directly related to plate material and thickness in which if bipolar plates were permeable to ions in electrolytes, internal short-circuiting can occur. To address this, Zhou et al. [45] used titanium bipolar plates (0.1 mm thickness) in their 19-cell stack to prevent this permeability. Evanko et al. [54] also recently investigated stackable bipolar pouch cells and suggested that lightweight carbon/polymer composite films can also be suitable as bipolar plates with a minimum thickness of 0.025 mm in which in their study, permeability testing

was conducted on carbon black/polyethylene composite films and showed very low electrolyte permeability in a HBr solution for 72 h. Alternatively, these researchers also reported that HBr can easily permeate through a 0.13-mm-thick sheet of expanded graphite in acidic solutions.

Although bipolar stacking designs can effectively reduce the total weight of energy storage stacks, the ESR of stacked cells also needs to be carefully considered. This is because as EES cells are connected in series, their ESR will sum up in the stack. Because manufacture inconsistency is not uncommon, cells with high ESR in the stack can cause distorted GCDs, leading to serious performance degradation [53, 55, 56]. Here, researchers have suggested that stack designs involving parallel cells can minimise increased ESR and maintain output voltage as a single cell [56].

Table 1 Summary of different charge storage mechanisms* in supercapacitors, supercapatteries, supercabatteries and batteries along with corresponding performance metrics of representative cells by using different types of electrolytes (aq.=the aqueous electrolyte, IL=the IL-based electrolyte, organic = the organic electrolyte)

Device	Supercapattery							Battery
	Supercapacitor		Hybrid				Others (supercabattery)	
	EDLC	Pseudocapacitor	Capacitive hybrid					
	NFCS + NFCS	NFCS + CFS	CFS + CFS	NFCS + NCFS	CFS + NCFS	NFCS + NCFS	CFS + NCFS	NFCS + NCFS
Electrode material								
Specific energy (Wh kg ⁻¹)	102 (IL), 6.7 (aq.)	3.6	26.6	230	261	–	208.6	250
Max specific power (W g ⁻¹)	111.6	24.7	13	59	25	–	3	1.5
Cycling life (cycles)	> 10000	> 5000	> 5000	> 1000	> 10000	–	> 1000	< 1200
Electrolyte types	IL, aq.	aq.	aq.	IL	IL	–	Organic	Organic
References	[57, 58]	[45]	[19]	[23, 59]	[60]	–	[22]	**

*NFCS: Non-Faradaic capacitive storage = electrical double-layer capacitance storage, CFS: capacitive Faradaic storage = pseudocapacitive storage, NCFS: non-capacitive faradaic storage = battery-type storage or Nernstian charge storage

**Data from web: https://en.wikipedia.org/wiki/Lithium-ion_battery#cite_note-7

5 Summary and Prospects of Supercapatteries

‘Supercapattery’ is a generic term to describe a large group of hybrid EES devices that can combine the merits of rechargeable batteries with the merits of supercapacitors (Table 1). In these supercapatteries, three charge storage mechanisms can be applied to describe and compare the performance of electrode materials, including non-Faradaic capacitive storage (EDL capacitance), capacitive Faradaic storage (pseudocapacitive storage) and non-capacitive Faradaic storage (battery-type storage or Nernstian charge storage). In addition, because redox electrolytes can also contribute to the energy storage of EDLCs, such EDLCs also fall in the scope of supercapatteries. As for scalable supercapatteries, the selections of electrode materials and electrode fabrication methods are of equal importance in the performance of resulting devices in which the bipolar stacking with multiple supercapattery cells can achieve high energy density storage due to the reduction in almost half of the auxiliary materials (current collectors) if the permeability of the bipolar plates is ensured.

Overall, supercapatteries have attracted increasing attention in the EES community based on the increasing number of publications using the expression ‘supercapattery’, which is a more accurate generic term to define various EES hybrids that can balance energy capacity with power capability in one device. Here, the development of battery and supercapacitor materials can benefit the development of supercapatteries. In addition, novel engineering designs for supercapatteries such as the bipolar stacking are required to

cross the gap between the laboratory setting and industrial manufacturing. Furthermore, more consideration needs to be given to the adaptive process for the manufacturing of supercapatteries using existing equipment for commercial batteries and supercapacitors.

Acknowledgements This work received funding from the Ningbo Municipal Government (3315 Plan and IAMET Special Fund, 2014A35001-1) and the Zhejiang Provincial Applied Research Programme for Commonweal Technology 2017C31104. Funding was provided by Engineering and Physical Sciences Research Council (Grant Nos. EP/J000582/1, GR/R68078).

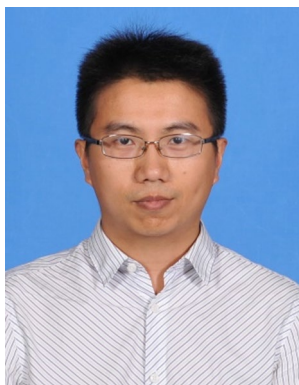
Open Access This article is licensed under a Creative Commons Attribution 4.0 International License, which permits use, sharing, adaptation, distribution and reproduction in any medium or format, as long as you give appropriate credit to the original author(s) and the source, provide a link to the Creative Commons licence, and indicate if changes were made. The images or other third party material in this article are included in the article’s Creative Commons licence, unless indicated otherwise in a credit line to the material. If material is not included in the article’s Creative Commons licence and your intended use is not permitted by statutory regulation or exceeds the permitted use, you will need to obtain permission directly from the copyright holder. To view a copy of this licence, visit <http://creativecommons.org/licenses/by/4.0/>.

References

1. Larcher, D., Tarascon, J.M.: Towards greener and more sustainable batteries for electrical energy storage. *Nat. Chem.* **7**, 19–29 (2015). <https://doi.org/10.1038/nchem.2085>
2. Shabangoli, Y., Rahmanifar, M.S., El-Kady, M.F., et al.: Thionine functionalized 3D graphene aerogel: combining simplicity and efficiency in fabrication of a metal-free redox supercapacitor.

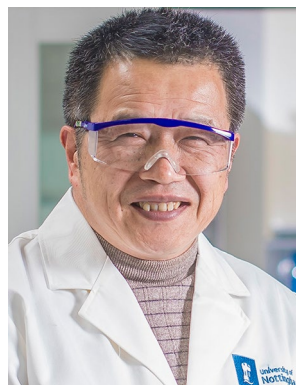
- Adv. Energy Mater. **8**, 1802869 (2018). <https://doi.org/10.1002/aenm.201802869>
3. Shang, W., Liu, Y., Kim, E., et al.: Selective assembly and functionalization of miniaturized redox capacitor inside microdevices for microbial toxin and mammalian cell cytotoxicity analyses. *Lab Chip* **18**, 3578–3587 (2018). <https://doi.org/10.1039/c8lc00583d>
 4. Byeon, A., Boota, M., Beidaghi, M., et al.: Effect of hydrogenation on performance of TiO₂(B) nanowire for lithium ion capacitors. *Electrochem. Commun.* **60**, 199–203 (2015). <https://doi.org/10.1016/j.elecom.2015.09.004>
 5. Chen, Z.K., Lang, J.W., Liu, L.Y., et al.: Preparation of a NbN/graphene nanocomposite by solution impregnation and its application in high-performance Li-ion hybrid capacitors. *RSC Adv.* **7**, 19967–19975 (2017). <https://doi.org/10.1039/c7ra01671a>
 6. Ma, Y., Chang, H., Zhang, M., et al.: Graphene-based materials for lithium-ion hybrid supercapacitors. *Adv. Mater.* **27**, 5296–5308 (2015). <https://doi.org/10.1002/adma.201501622>
 7. Shen, L., Lv, H., Chen, S., et al.: Peapod-like Li₃VO₄/N-doped carbon nanowires with pseudocapacitive properties as advanced materials for high-energy lithium-ion capacitors. *Adv. Mater.* **29**, 1700142 (2017). <https://doi.org/10.1002/adma.201700142>
 8. Wang, H., Zhu, C., Chao, D., et al.: Nonaqueous hybrid lithium-ion and sodium-ion capacitors. *Adv. Mater.* **29**, 1702093 (2017). <https://doi.org/10.1002/adma.201702093>
 9. Arnaiz, M., Gomez-Camer, J.L., Ajuria, J., et al.: High performance titanium antimonide TiSb₂ alloy for Na-ion batteries and capacitors. *Chem. Mater.* **30**, 8155–8163 (2018). <https://doi.org/10.1021/acs.chemmater.8b02639>
 10. Thangavel, R., Kaliyappan, K., Kim, D.U., et al.: All-organic sodium hybrid capacitor: a new, high-energy, high-power energy storage system bridging batteries and capacitors. *Chem. Mater.* **29**, 7122–7130 (2017). <https://doi.org/10.1021/acs.chemmater.7b00841>
 11. Cherusseri, J., Sambath Kumar, K., Choudhary, N., et al.: Novel mesoporous electrode materials for symmetric, asymmetric and hybrid supercapacitors. *Nanotechnology* **30**, 202001 (2019). <https://doi.org/10.1088/1361-6528/ab0685>
 12. Makino, S., Shinohara, Y., Ban, T., et al.: 4 V class aqueous hybrid electrochemical capacitor with battery-like capacity. *RSC Adv.* **2**, 12144–12147 (2012). <https://doi.org/10.1039/c2ra22265e>
 13. Rafai, S., Qiao, C., Naveed, M., et al.: Microwave-anion-exchange route to ultrathin cobalt-nickel-sulfide nanosheets for hybrid supercapacitors. *Chem. Eng. J.* **362**, 576–587 (2019). <https://doi.org/10.1016/j.cej.2019.01.059>
 14. Xie, L.Y., Zong, Q.J., Zhang, Q.C., et al.: Hierarchical NiCoP nanosheet arrays with enhanced electrochemical properties for high-performance wearable hybrid capacitors. *J. Alloys Compd.* **781**, 783–789 (2019). <https://doi.org/10.1016/j.jallcom.2018.12.067>
 15. Zuo, W., Li, R., Zhou, C., et al.: Battery-supercapacitor hybrid devices: recent progress and future prospects. *Adv. Sci.* **4**, 1600539 (2017). <https://doi.org/10.1002/advs.201600539>
 16. Li, H.B., Yu, M.H., Wang, F.X., et al.: Amorphous nickel hydroxide nanospheres with ultrahigh capacitance and energy density as electrochemical pseudocapacitor materials. *Nat. Commun.* **4**, 1894 (2013). <https://doi.org/10.1038/ncomms2932>
 17. Nam, K.W., Ma, S.B., Yoon, W.S., et al.: Novel concept of pseudocapacitor using stabilized lithium metal powder and non-lithiated metal oxide electrodes in organic electrolyte. *Electrochem. Commun.* **11**, 1166–1169 (2009). <https://doi.org/10.1016/j.elecom.2009.03.038>
 18. Wu, C., Lu, X., Peng, L., et al.: Two-dimensional vanadyl phosphate ultrathin nanosheets for high energy density and flexible pseudocapacitors. *Nat. Commun.* **4**, 2431 (2013). <https://doi.org/10.1038/ncomms3431>
 19. Huang, Z.H., Song, Y., Xu, X.X., et al.: Ordered polypyrrole nanowire arrays grown on a carbon cloth substrate for a high-performance pseudocapacitor electrode. *ACS Appl. Mater. Inter.* **7**, 25506–25513 (2015). <https://doi.org/10.1021/acsami.5b08830>
 20. Peng, X., Chai, H., Cao, Y.L., et al.: Facile synthesis of cost-effective Ni₃(PO₄)₂·8H₂O microstructures as a supercapattery electrode material. *Mater. Today Energy* **7**, 129–135 (2018). <https://doi.org/10.1016/j.mtener.2017.12.004>
 21. Raj, S., Kar, P., Roy, P.: Facile synthesis of flower-like morphology Cu_{0.27}Co_{2.73}O₄ for a high-performance supercapattery with extraordinary cycling stability. *Chem. Commun.* **54**, 12400–12403 (2018). <https://doi.org/10.1039/c8cc04625e>
 22. Zhou, H.T., Wang, X.H., Sheridan, H., et al.: Boosting the energy density of 3D dual-manganese oxides-based li-ion supercapattery by controlled mass ratio and charge injection. *J. Electrochem. Soc.* **163**, A2618–A2622 (2016). <https://doi.org/10.1149/2.0691613jes>
 23. Yu, L., Chen, G.Z.: High energy supercapattery with an ionic liquid solution of LiClO₄. *Faraday Discuss.* **190**, 231–240 (2016). <https://doi.org/10.1039/c5fd00232j>
 24. Akinwolemiwa, B., Wei, C.H., Yang, Q.H., et al.: Optimal utilization of combined double layer and Nernstian charging of activated carbon electrodes in aqueous halide supercapattery through capacitance unequalization. *J. Electrochem. Soc.* **165**, A4067–A4076 (2018). <https://doi.org/10.1149/2.0031902jes>
 25. Akinwolemiwa, B., Chen, G.Z.: Fundamental consideration for electrochemical engineering of supercapattery. *J. Braz. Chem. Soc.* **29**, 960–972 (2018). <https://doi.org/10.21577/0103-5053.20180010>
 26. Xia, L., Yu, L.P., Hu, D., et al.: Electrolytes for electrochemical energy storage. *Mater. Chem. Front.* **1**, 584–618 (2017). <https://doi.org/10.1039/c6qm00169f>
 27. Chen, G.Z.: Supercapacitor and supercapattery as emerging electrochemical energy stores. *Int. Mater. Rev.* **62**, 173–202 (2017). <https://doi.org/10.1080/09506608.2016.1240914>
 28. Akinwolemiwa, B., Wei, C.H., Chen, G.Z.: Mechanisms and designs of asymmetrical electrochemical capacitors. *Electrochim. Acta* **247**, 344–357 (2017). <https://doi.org/10.1016/j.electacta.2017.06.088>
 29. Yu, L.P., Chen, G.Z.: Redox electrode materials for supercapatteries. *J. Power Sources* **326**, 604–612 (2016). <https://doi.org/10.1016/j.jpowsour.2016.04.095>
 30. Guan, L., Yu, L.P., Chen, G.Z.: Capacitive and non-capacitive faradaic charge storage. *Electrochim. Acta* **206**, 464–478 (2016). <https://doi.org/10.1016/j.electacta.2016.01.213>
 31. Chen, G.Z.: Understanding supercapacitors based on nano-hybrid materials with interfacial conjugation. *Progress Nat. Sci. Mater. Int.* **23**, 245–255 (2013). <https://doi.org/10.1016/j.pnsc.2013.04.001>
 32. Chae, J.H., Chen, G.Z.: 1.9 V aqueous carbon-carbon supercapacitors with unequal electrode capacitances. *Electrochim. Acta* **86**, 248–254 (2012). <https://doi.org/10.1016/j.electacta.2012.07.033>
 33. Demarconnay, L., Raymundo-Piñero, E., Béguin, F.: A symmetric carbon/carbon supercapacitor operating at 1.6 V by using a neutral aqueous solution. *Electrochem. Commun.* **12**, 1275–1278 (2010). <https://doi.org/10.1016/j.elecom.2010.06.036>
 34. Khomenko, V., Raymundo-Piñero, E., Béguin, F.: Optimisation of an asymmetric manganese oxide/activated carbon capacitor working at 2 V in aqueous medium. *J. Power Sources* **153**, 183–190 (2006). <https://doi.org/10.1016/j.jpowsour.2005.03.210>
 35. Bard, A.J., Faulkner, L.R.: *Electrochemical Methods: Fundamentals and Applications*. Wiley, New York (2001)
 36. Hu, D., Peng, C., Chen, G.Z.: Electrodeposition of nonconducting polymers: roles of carbon nanotubes in the process and products. *ACS Nano* **4**, 4274–4282 (2010). <https://doi.org/10.1021/nn100849d>

37. Peng, C., Jin, J., Chen, G.Z.: A comparative study on electrochemical co-deposition and capacitance of composite films of conducting polymers and carbon nanotubes. *Electrochim. Acta* **53**, 525–537 (2007). <https://doi.org/10.1016/j.electacta.2007.07.004>
38. Che, C.Y., Vagin, M., Ail, U., et al.: Twinning lignosulfonate with a conducting polymer via counter-ion exchange for large-scale electrical storage. *Adv. Sustain. Syst.* **3**, 9 (2019). <https://doi.org/10.1002/adsu.201900039>
39. Lee, H.W., Shinde, N.M., Shinde, P.V., et al.: High energy and power density of self-grown CuS@Cu₂O core-shell supercapattery positrode. *J. Solid State Electrochem.* **23**, 2609–2617 (2019). <https://doi.org/10.1007/s10008-019-04351-0>
40. Priyadharsini, N., Shanmugavani, A., Surendran, S., et al.: Improved electrochemical performances of LiMnPO₄ synthesized by a hydrothermal method for Li-ion supercapatteries. *J. Mater. Sci. Mater. Electron.* **29**, 18553–18565 (2018). <https://doi.org/10.1007/s10854-018-9972-5>
41. Shinde, N.M., Xia, Q.X., Yun, J.M., et al.: Polycrystalline and Mesoporous 3-D Bi₂O₃ nanostructured negatodes for high-energy and power-asymmetric supercapacitors: superfast room-temperature direct wet chemical growth. *ACS Appl. Mater. Inter.* **10**, 11037–11047 (2018). <https://doi.org/10.1021/acsami.8b00260>
42. Sun, X.W., Simonsen, S.C., Norby, T., et al.: Composite membranes for high temperature PEM fuel cells and electrolyzers: a critical review. *Membranes* **9**, 46 (2019). <https://doi.org/10.3390/membranes9070083>
43. Surendran, S., Shanmugapriya, S., Zhu, P., et al.: Hydrothermally synthesised NiCoP nanostructures and electrospun N-doped carbon nanofiber as multifunctional potential electrode for hybrid water electrolyser and supercapatteries. *Electrochim. Acta* **296**, 1083–1094 (2019). <https://doi.org/10.1016/j.electacta.2018.11.078>
44. Xia, Q.X., Shinde, N.M., Zhang, T.F., et al.: Seawater electrolyte-mediated high volumetric MXene-based electrochemical symmetric supercapacitors. *Dalton Trans.* **47**, 8676–8682 (2018). <https://doi.org/10.1039/c8dt01375f>
45. Zhou, X.H., Peng, C., Chen, G.Z.: 20 V stack of aqueous supercapacitors with carbon (–), titanium bipolar plates and CNT-polypyrrole composite (+). *AIChE J.* **58**, 974–983 (2012). <https://doi.org/10.1002/aic.12632>
46. Jin, X., Zhou, W., Zhang, S., et al.: Nanoscale microelectrochemical cells on carbon nanotubes. *Small* **3**, 1513–1517 (2007). <https://doi.org/10.1002/sml.200700139>
47. Akinwolemiwa, B., Peng, C., Chen, G.Z.: Redox electrolytes in supercapacitors. *J. Electrochem. Soc.* **162**, A5054–A5059 (2015). <https://doi.org/10.1149/2.0111505jes>
48. Evanko, B., Boettcher, S.W., Yoo, S.J., et al.: Redox-enhanced electrochemical capacitors: status, opportunity, and best practices for performance evaluation. *ACS Energy Lett.* **2**, 2581–2590 (2017). <https://doi.org/10.1021/acsenerylett.7b00828>
49. Lee, J., Srimuk, P., Fleischmann, S., et al.: Redox-electrolytes for non-flow electrochemical energy storage: a critical review and best practice. *Prog. Mater. Sci.* **101**, 46–89 (2019). <https://doi.org/10.1016/j.pmatsci.2018.10.005>
50. Mourad, E., Coustan, L., Lannelongue, P., et al.: Biredox ionic liquids with solid-like redox density in the liquid state for high-energy supercapacitors. *Nat. Mater.* **16**, 446–453 (2017). <https://doi.org/10.1038/nmat4808>
51. Peng, C., Hu, D., Chen, G.Z.: Achieving low voltage half electrolysis with a supercapacitor electrode. *Energy Environ. Sci.* **7**, 1018–1022 (2014). <https://doi.org/10.1039/c3ee43817a>
52. Peng, C., Snook, G.A., Fray, D.J., et al.: Carbon nanotube stabilised emulsions for electrochemical synthesis of porous nanocomposite coatings of poly[3,4-ethylene-dioxythiophene]. *Chem. Commun.* **44**, 4629–4631 (2006). <https://doi.org/10.1039/b609293d>
53. Zhou, X.H., Chen, G.Z.: Electrochemical performance of screen-printed composite coatings of conducting polymers and carbon nanotubes on titanium bipolar plates in aqueous asymmetrical supercapacitors. *J. Electrochem.* **18**, 548–565 (2012)
54. Evanko, B., Yoo, S.J., Lipton, J., et al.: Stackable bipolar pouch cells with corrosion-resistant current collectors enable high-power aqueous electrochemical energy storage. *Energy Environ. Sci.* **11**, 2865–2875 (2018). <https://doi.org/10.1039/c8ee00546j>
55. Kaipannan, S., Marappan, S.: Fabrication of 9.6 V high-performance asymmetric supercapacitors stack based on nickel hexacyanoferrate-derived Ni(OH)₂ nanosheets and bio-derived activated carbon. *Sci. Rep.* **9**, 1 (2019). <https://doi.org/10.1038/s41598-018-37566-8>
56. Li, J.M., Kurra, N., Seredych, M., et al.: Bipolar carbide-carbon high voltage aqueous lithium-ion capacitors. *Nano Energy* **56**, 151–159 (2019). <https://doi.org/10.1016/j.nanoen.2018.11.042>
57. Hou, J., Cao, C., Idrees, F., et al.: Hierarchical porous nitrogen-doped carbon nanosheets derived from silk for ultrahigh-capacity battery anodes and supercapacitors. *ACS Nano* **9**, 2556–2564 (2015). <https://doi.org/10.1021/nn506394r>
58. Lewandowski, A., Olejniczak, A., Galinski, M., et al.: Performance of carbon-carbon supercapacitors based on organic, aqueous and ionic liquid electrolytes. *J. Power Sources* **195**, 5814–5819 (2010). <https://doi.org/10.1016/j.jpowsour.2010.03.082>
59. Zhang, F., Zhang, T.F., Yang, X., et al.: A high-performance supercapacitor-battery hybrid energy storage device based on graphene-enhanced electrode materials with ultrahigh energy density. *Energy Environ. Sci.* **6**, 1623–1632 (2013). <https://doi.org/10.1039/c3ee40509e>
60. Ortaboy, S., Alper, J.P., Rossi, F., et al.: MnO_x-decorated carbonized porous silicon nanowire electrodes for high performance supercapacitors. *Energy Environ. Sci.* **10**, 1505–1516 (2017). <https://doi.org/10.1039/c7ee00977a>



Linpo Yu is a Senior Research Fellow in Electrochemistry at the University of Nottingham Ningbo China. He is a member of the Royal Society of Chemistry. He received his BS in chemistry and PhD in physical chemistry (electrochemistry) from Wuhan University in 2003 and 2008, respectively. He was a Research Assistant at Suzhou Institute of Nano-Tech and Nano-Bionics, CAS, from 2008 to 2013. Then, he carried out his postdoctoral research at the University of Nottingham in the UK

for 2 years until he joined in the University of Nottingham Ningbo China in 2015. His main research interests include the supercapacitor and supercapattery electrode materials, ionic liquid electrolytes and thermochromic materials.



George Zheng Chen, CChem, FRSC, FRSA, FIMMM is a professor of electrochemical technologies in both the Nottingham and Ningbo campuses of the University of Nottingham. He received both his Teaching Diploma (1981, Jiujiang Teacher Training College) and MSc (1985, Fujian Normal University, Prof. Qixin Zhang) in China. After obtaining his PhD in 1992 from University of London (Imperial College, Prof. John Albery, FRS), he worked in the Universities of Oxford (1992–1994), Leeds

(1994–1996) and Cambridge (1996–2003, Darwin). He also undertook academic duties in Jiangxi University (1985–1988) and Wuhan University (2000–2010, invited position). His research aims at electrochemical and liquid salt innovations for materials, energy and environment, producing 700+ documented outputs, including the Fray-Farthing-Chen Cambridge Process.